Investigation of active faulting at the Emigrant Peak fault in Nevada using shallow seismic reflection and ground penetrating radar

by

Michael Wayne Christie
B.S., University of Kansas, 2005

Submitted to the Department of Geology
and the Faculty of the Graduate School of the University of Kansas
in partial fulfillment of the requirements for the degree of
Master of Science

_____
Dr. George Tsoflias, Chairman

_____
Dr. Ross Black, Committee Member

_____
Dr. Daniel Stockli, Committee Members

Date Defended _____

The Thesis Committee for Michael Christie certifies
That this is the approved version of the following thesis:

Investigation of active faulting at the Emigrant Peak fault in Nevada using shallow seismic reflection and ground penetrating radar

Committee:

_____
Dr. George Tsoflias, Chairman

_____
Dr. Ross Black, Committee Member

_____
Dr. Daniel Stockli, Committee Members

Date approved: _____

Abstract

The objective of this study was to assess fault displacement, off-fault deformation, and alluvial fan stratigraphy at the Emigrant Peak fault zone (EPFZ) in Fish Lake Valley, Nevada utilizing shallow seismic reflection (SSR) and ground penetrating radar (GPR) geophysical imaging methods. A three-dimensional higher frequency GPR survey provided high resolution imaging of the top 25 meters. Two-dimensional SSR and lower frequency GPR profiles imaged the subsurface at depths ranging from 20-225 m and 4-40 m respectively. Both the SSR and GPR data revealed structural geometries dominated by NW-dipping normal faulting and corresponding antithetic faults with identifiable offsets. Near the main fault strand, alluvial fan strata dip consistently to the NW while the stratigraphic architecture becomes more complex in the down-dip direction, including colluvial wedges and small graben structures. Diffuse faulting was identified tens to hundreds of meters away from the main fault, both in the footwall and hanging wall blocks.

Acknowledgements

I would like to thank Ryan Brumbaugh, Kwan Yee Cheng, Nazim Louni, and Brian Miller for assistance in field data acquisition. I also would like to thank John Lee for acquiring the DGPS data and Jeff Schroeder for his neotectonic insights and sharing unpublished neotectonic mapping. The work would not have been possible without the help of my adviser, Dr. George Tsoflias, and committee members Drs. Ross Black and Daniel Stockli. All three not only aided with writing and data processing and interpretation, but collected the data in the field as well.

Table of Contents

List of Figures

Introduction

The use of high-resolution geophysical imaging techniques, including ground penetrating radar (GPR) and shallow seismic reflection (SSR), is becoming a more common practice in the characterization of fault zones. These geophysical methods allow for characterization of the subsurface on a meter to sub-meter scale resolution and are non-invasive, compared to more traditional methods such as trenching and drilling. For imaging fault zones, geophysical methods provide a more comprehensive view of the subsurface and a greater areal extent than the other methods. In conjunction with geologic and neotectonic mapping, geochronology techniques, GPS studies of strain rates, and paleoseismic trenching studies, these geophysical techniques can add a wealth of knowledge to the study of fault zones.

The use of GPR and SSR investigations can enhance the previously mentioned techniques in a number of ways. Geologic and neotectonic mapping are both important tools used to aid in the understanding of fault systems and individual fault zones; they provide the information for identifying faults in the field. The geophysical techniques extend the capabilities of surface methods by adding the component of subsurface mapping to the knowledge bank for a given fault zone. Trenching and drilling provide the highest possible vertical resolution for understanding a given fault zone though they are invasive, have limited areal coverage, and are generally costly. With this in mind, a preliminary picture of the subsurface generated from GPR or SSR can help optimize the positioning of

trenches and wells that can add important information to the characterization of a fault zone. The geophysical techniques could also provide insight into the stratigraphy and hence the depositional environments that likely contain the type of samples necessary for geochronological dating techniques. Providing information helpful in determining off-fault deformation is one of the more important uses for GPR and SSR. This is important when trying to compare geologic deformation rates to deformation rates determined by geodetic studies. Geophysical imaging can aid in determining the deformation associated with a fault that may not be evident from surface mapping. When the geodetic rates are higher than the determined geologic rates, off-fault deformation can be one of the means by which to reconcile the difference.

The objective of this project is to use GPR and SSR techniques to better characterize the Emigrant Peak fault zone in Fish Lake Valley, Nevada. Some of the information sought using these geophysical techniques included the feasibility of imaging the associated alluvial fan, the stratigraphy in the alluvial fan, the location of the fault at depth, and the structures associated with the main fault (unmapped fault strands, other deformational features, colluvial wedge deposition, and stratigraphic changes associated with faulting). The data gathered for this study will also be used in conjunction with more conventional geologic mapping and geochronologic studies.

The GPR study has two main components, a quasi (non-regular) 3-D dataset and a longer 2-D line. The SSR portion includes two common midpoint

(CMP) surveys, a longer inline and a shorter cross-line. The premise for using both techniques is to gain a more complete image of the subsurface. GPR generally images to a depth of 10 to 20 m but can image depths greater than 40 m in low electrical conductivity environments (Davis & Annan, 1989). SSR can image a range of depths, but this study was aimed at imaging the upper few hundred meters of the subsurface. The combination of the techniques allows for a subsurface image from the surface to a depth of a few hundred meters.

This type of study has been undertaken before in other locations around the world on various types of faults and geologic settings with varying amounts of success and data quality. One of the earlier studies using high-resolution seismic reflection techniques was done by Sexton and Jones (1986). They looked for evidence of recurrent faulting in the New Madrid seismic zone. They were able to image reflectors that are vertically offset and from this, came to conclusions about the amount of offset for at least the portion of the faults they identified. The resolution was much less than that which this study entails. Sexton and Jones' survey used greater geophone and shot point spacing as well as survey line length that allowed for greater depth of investigation (> 500 m) but far less vertical and horizontal resolution. The study was important in that it allowed for better understanding of a structure that was not apparent from surficial geologic mapping. Later studies have used both GPR and SSR to gain a more complete image of the subsurface (Bano, et al. 2002; Chow, et al. 2001; Demanet, et al. 2001; Rashed and Nakagawa 2004). In the cases where GPR and SSR were

combined, the lines were generally of unequal quality and lacked any spatial overlap in imaging. All of the cases used offset reflectors or changes in reflector nature (amplitude, continuity) to discern faults in the subsurface. The radar surveys generally imaged 10 m into the subsruface while the seismic surveys imaged several hundred meters. They had a stark contrast in resolution which prohibited integration of the two methods into a single, relatively coherent image. These studies also used single 2-D lines which limited the ability to construct a three-dimensional image of the faults and associated stratigraphy. Gross et al. 2004 and Gross et al. 2002 both took advantage of 3-D radar surveys to investigate two strike-slip faults, the Wellington (New Zealand) and San Andreas (California) faults respectively. The data for the Wellington survey imaged to depths of ~20 m and provided clear indications of the fault zone. Some of the reflectors within the fault zone were parallel to the orientation of the fault itself. The survey collected at the San Andreas Fault imaged to a depth of ~4.5 m. The fault zone was primarily identified by discontinuous reflectors. A more important observation for the survey, however, was the imaging of a feature that showed 4.5-5.5 m of right-lateral movement. Though GPR and SSR surveys have been employed to aid in the identification of faults in the subsurface, this project is unique when compared to prior studies. One of the main objectives of this study was to image the active alluvial fan associated with the EPFZ with GPR and SSR, something that has not been presented in the literature (Mills and Speece 1997, Ekes and Hickin 2001). The second objective is to use these geophysical tools in

order to image the Emigrant Peak fault zone. Imaging the fault zone includes the alluvial fan stratigraphy, the main fault itself, other deformational features including fault strands that may not have a surface expression, and any possible depositional responses to faulting indicated by alluvial fan stratigraphy. In order to accomplish these objectives, we acquired the largest 3-D GPR survey and highest resolution SSR data reported in the study of fault zones. The geophysical data were of comparable resolution which allowed combining them into a single interpretation and obtain a comprehensive image of the subsurface where the data allowed; information about offset (amount, possible strike-slip component, number of events, etc.) was determined. This data can then be compared with the geologic information gathered in the field to construct a copmrehensive view of the fault zone.

Geologic Setting

Emigrant Peak Fault, Eastern California Shear Zone and Walker Lane Belt

The Emigrant Peak fault is a normal fault located at the northern end of Fish Lake Valley, Nevada (figure 1). The Emigrant Peak fault is a step-over associated with the larger Death Valley-Furnace Creek-Fish Lake Valley fault system (DV-FC-FLV) (figure 2). On the larger scale the fault system is associated with the central Walker Lane Belt (WLB) and the Eastern California Shear Zone (ECSZ) (Reheis & Sawyer, 1997). The WLB and ECSZ are related to

the North American-Pacific plate motion. Though the San Andreas fault accomodates the majority of the relative plate motion, approximately 25% is accomodated by the ECSZ and WLB (Wesnousky, 2005). The San Andreas fault system is transpressional and the ECSZ and WLB represent a

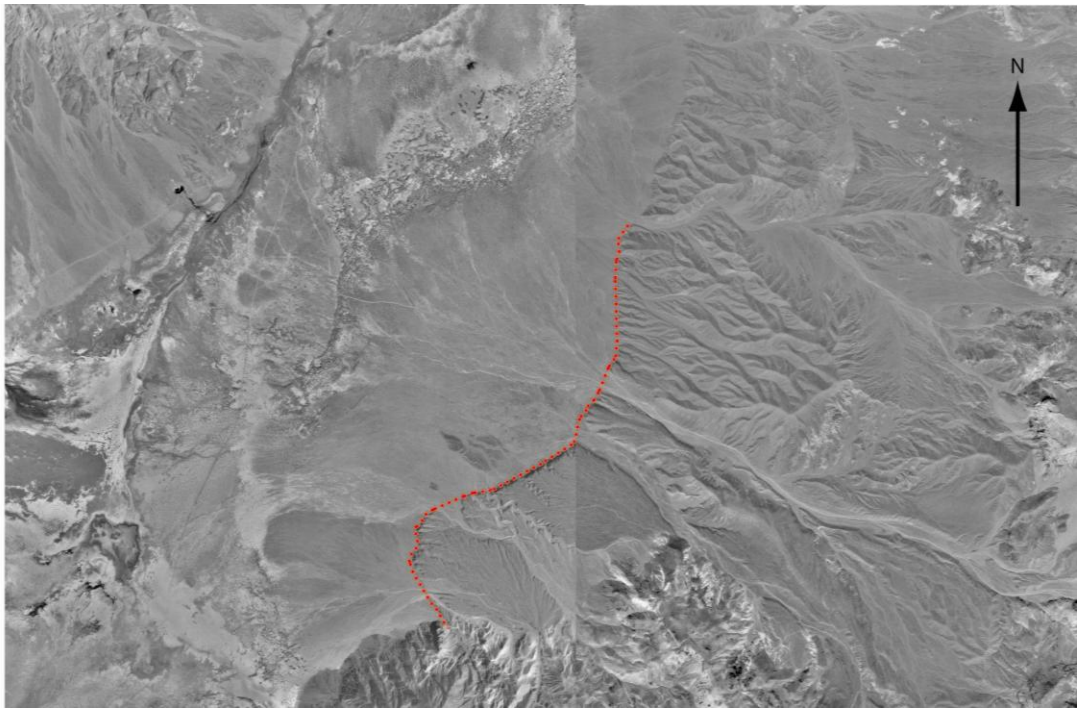

Figure 1. Aerial photograph of the EMPZ. The red, dashed line represents the location of the present fault scarp.

transtensional environment (Wesnousky, 2005). The ECSZ and WLB consist of a series of northwest striking, dextral strike-slip faults with normal faults that accommodate extension in the region (figure 2). The WLB and ECSZ act as a transitional zone between the plate boundary and the extensional Basin and Range province. The Fish Lake Valley (FLV) fault and Emigrant Peak fault are on the western edge of the central WLB. The Mina Deflection, in the central WLB,

links the NW-trending faults of the central Walker Lane to the NW-trending faults of the Owens Valley - Fish Lake Valley fault system by transferring displacement in an extensional right-step along a system of E-W striking faults (Petronis, 2005).

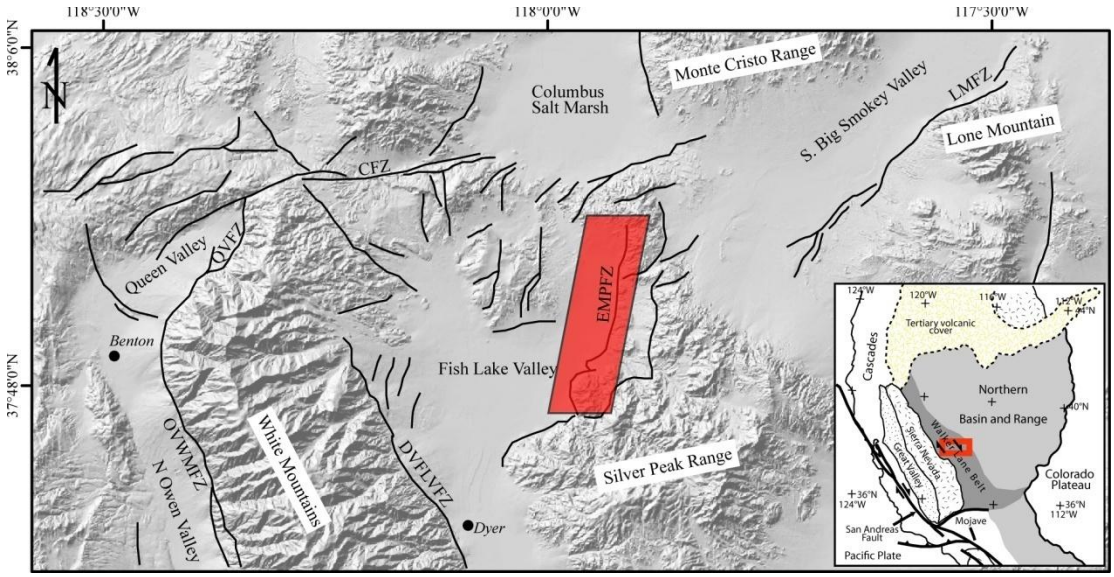

Figure 2. Digital shaded-relief map of west-central Nevada and east-central California, showing major late Cenozoic faults (modified after Oldow 1992, Stockli, et al. 2003). The shaded box represents the area shown in figure 1. Map key: OVWMFZ, Owens Valley-White Mountain fault zone; QVFZ, Queen Valley fault zone; CFZ, Coaldale fault zone; DVFCFLVFZ, Death Valley-Furnace Creek-Fish Lake Valley fault zone; EMPFZ, Emigrant Peak fault zone; LMFZ, Lone Mountain fault zone.

Motion on the right-lateral FLV fault initiated approximately 10 Ma and the long-term lateral slip rate is approximately 5 mm/yr. The overall FLV fault zone rate of 10-12 mm/yr accounts for nearly half of the North American-Pacific

plate boundary motion accommodated in the Basin and Range tectonic province (Reheis & Sawyer, 1997).

The Emigrant Peak fault zone (EPFZ) is comprised of north-striking normal faults that offset Pliocene and Quaternary deposits (Reheis & Sawyer, 1997). Reheis and Sawyer (1997) used offset tephra beds and surface offsets of alluvial fan surfaces in order to arrive at slip rate estimates for the fault zone. The tephra deposits used to determine offset and slip rate at the fault zone have yielded preferred results of 410 m offset for a slip rate of 0.21 mm/yr. The base of an alluvial gravel layer yields results of 635 to 800 m of offset and corresponding slip rates of 0.19 to 0.40 mm/yr. Alluvial fan surface units showed offsets of 30 to 60 m and 20 to 26 m with slip rates of 0.40 to 1.3 mm/yr and 2.5 to 5.2 mm/yr, respectively (Reheis & Sawyer, 1997). The alluvial fan surface units represent late quaternary rates. The quaternary rates are higher than what is normally seen for faults of the Basin and Range, though this increased rate is likely related to the high lateral-slip rates associated with the FLV fault zone (Reheis & Sawyer, 1997). Reheis and Sawyer (1997), have estimated that the dip of faults in the fault zone range from 45° to 70° from east to west, which they predicate to westward propogation of the fault zone over time.

The EPFZ is thought to have aided in the extension and creation of the valley in northeastern FLV. The initiation of faulting is coeval with opening of northern FLV and began approximately 5 Ma (Reheis & Sawyer, 1997). This timing follows the proposed timing for the displacement on the shallowly dipping

Silver Peak-Lone Mountain detachment system from 11 to 6 Ma (Oldow, et al. 1994). The Silver Peak-Lone Mountain detachment is thought to have accomodated 8-15 km of NW extension (Diamond & Ingersoll, 2002). The detachment is thought to link the DV-FC-FLV fault system to the central Walker Lane strike-slip faults, and the EPFZ represents part of the upper-plate extension associated with the detachment fault (Oldow, et al. 1994). With this in mind, it is assumed that the EMPZ soles into the detachment at depth (approximately 1 km) or it completely cuts through the detachment and soles into a fault elsewhere.

Local Geology of Emigrant Peak fault zone

The stratigraphy, or sedimentology at the fault zone that is of main interest to this study is that of the alluvial fan that is shed from the Silver Peak Range. Alluvial fan depostional architecture and changes in deposition associated with faulting on the Emigrant Peak fault are the main depositional features that the GPR and shallow seismic surveys imaged. Therefore, it is important to understand how the alluvial fan deposits were created, i.e. stream flows or debris flows, and the sedimentological characterization of each of the processes. In the seismic surveys, the depth of imaging may be great enough to see the pluvial lake sediments in northern FLV.

Bull (1977), describes an alluvial fan as a depostit whose surface forms a segment of a cone that radiates downslope from the point where a stream leaves its source area. The alluvial fans in FLV vary from unsorted, bouldery matrix-supported to moderately well-sorted, pebbly clast-supported deposits, though

most deposits fall within those two endmembers (Slate, 1992). The two main modes of deposition for the alluvial fans in FLV are debris flow deposits and stream flow deposits, with debris flows as the dominant means of sedimentation. Hooke (1967), describes debris flow and stream flow by both types being formed by water moving over and entraining loose sediment, but the difference lies at the point where sediment entrainment becomes irreversible. Streams can deposit their sediment load and continue flowing, while debris flows move by means of the entrained sediment; it follows that sediment flow ends when the load has been completely deposited. Most water-laid sediments in alluvial fans consist of sheets of sand, silt, and gravel that are deposited by braided distributary channels (Bull, 1977). Debris flows are characterized by being able to transport larger sediments such as cobbles and boulders, which helps to distinguish debris flow deposits from stream deposits.

The alluvial fan at EPFZ has not been characterized as extensively as fans in adjacent areas. Other alluvial fan deposits in FLV will be used as analogs for the geophysical study of the alluvial fan at EPFZ. Slate (1992), did an extensive study of alluvial fans at FLV and her work will be used to help distinguish characteristics observed on the alluvial fan at EPFZ. The alluvial fan at EPFZ is a debris-flow dominated alluvial fan. This is illustrated by the types of desposits present. The fan exhibits successions of matrix-supported (debris flow) deposits that exhibit a crude graded bedding which is high clast versus low clast composition (Slate, 1992).

Figure 3. Cross-sectional image of the makeup of the imaged alluvial fan (looking NNE). The red arrow points to a boulder that is approximately 1 meter in length. The blue arrow points to a scour surface likely created by debris flow movement. One can also notice the difference in grain size present; just above the boulder the grains are sand sized, while cobbles are present through the deposit.

Debris flows generally form when there is an accumulation of sediment and clasts within the drainage canyon and events such as a flash flood remove the debris from the canyon and transport it onto the alluvial fan (Beaty, 1963). At the time of deposition, debris flows have flat tops, steep sides, and a lobate form; after time, generally the cobble and boulder accumulations with low relief are what remain, an example of which can be seen in figure 4 (Hooke, 1967). Coarse material accumulates at the front of the debris flow and gets pushed to the side by the advancing flow; this forms levees along the sides. These debris flows tend to have pebbles on the inside and coarser material on the outer edges of the flows (Hooke, 1967).

Figure 4. EMFZ alluvial fan (looking towards the White Mountains), illustrating the low relief of the fan and large boulders that remain from likely debris flows.

The climate in the region results in debris flows being the dominant form of alluvial fan sedimentation. FLV is in an arid climate, and deposition will come with storms that create flooding events or run-off from snow melt, which are conducive to debris flow generation. Though debris-flow deposition is the dominate mode of deposition, stream-flow deposits play an important part as well.

Another important depositional process that is present at this alluvial fan and must be addressed is the formation of colluvial wedges. Colluvium is the unconsolidated material that is often found at the base of steep slopes. The grains are generally more angular than stream deposits because the grains have not been transported very far. Following the formation of a fault scarp generated by an earthquake, the exposed or free face will generally degrade into a debris slope that can give rise to a colluvial wedge (Keller & Pinter, 2002). There are generally

two main elements to a colluvial wedge: wash derived and debris derived (Nelson, 1992). Identifying these two types of deposits is useful when trying to interpret a colluvial wedge in the geophysical data. The debris facies is formed from the initial debris falling away from the free face and usually represents the base of the colluvial wedge (Nelson, 1992). After the dissappearance of the free face, colluvium deposited by wash processes are deemed the wash facies. This would also include the normal alluvial fan deposition (Nelson, 1992). The colluvial wedge deposition adds complexity to the already complex nature of the alluvial fan deposition, but being able to distinguish the colluvial wedge from surrounding sediments is an important part of identifying the stratigraphy of the alluvial fan and characterizing the fault zone.

There are other deposits that may be of interest to this study, such as pluvial lake deposits and possibly some volcanic ash deposits. A pluvial lake existed in FLV during the late Pliocene to middle Pleistocene (Reheis, et al. 1993). Figure 5 shows the pluvial lake shoreline extending to the EPFZ. It may be possible that some of the lake deposits may be imaged while investigating the alluvial fan. North of the survey area defined for this study, Reheis et al. (1993), found 15 m of white Bishop ash and lapilli that overlies indurated cobble-sized sandy fan gravel of volcanic and sedimentary rocks. The bed contains alternating layers of sand and fine gravel that have been interpreted to be indicative of beach sand, which gives this area a very shallow water level during deposition (Reheis, et al. 1993). There are a couple of caveats that must be understood when relating

this data to the specific site that was used for this study. The site of Reheis, et al. (1993) is north of the site for this study and since the pluvial lake was very shallow at that location, it is unknown if these lacustrine deposits are in the stratigraphic record at the EPFZ; and if so whether or not they could be imaged with the techniques being applied. When interpretation of the data takes place, the location and characteristics of the lacustrine deposits must be taken into consideration.

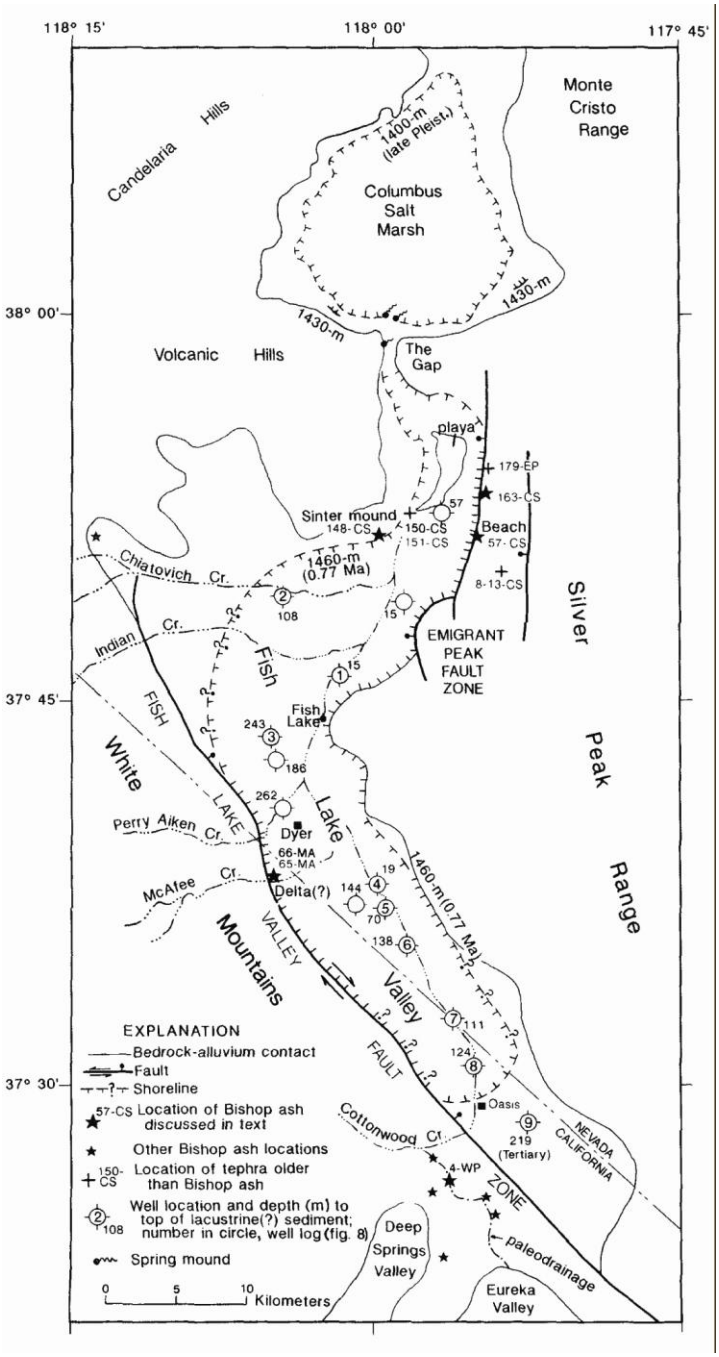

Figure 5. Map of the shoreline for the pluvial lake that existed in FLV. One can see that the shoreline is on the Emigrant Peak fault (from Reheis et. al, 1993).

Three-dimensional GPR imaging of off-fault deformation at Emigrant Peak Fault Zone

Introduction

Ground-penetrating radar (GPR) can provide images of the subsurface at meter to sub-meter scale resolution in a non-invasive and cost effective fashion when compared to other methods (such as drilling and trenching). Common techniques employed in fault zone studies have included, for example, geologic and neotectonic surface mapping, detailed paleoseismological trenching, and geodetic strain rate studies. GPR studies have the unique capability of providing high-resolution characterization of fault zones in three dimensions (3-D), allowing for a more representative and comprehensive investigation of near-surface structures and their spatial variations.

GPR surveys have been used to image faults and document off-fault deformation in varying geologic settings (Bano et al., 2002; Chow et al., 2001; Demanet et al., 2001; Rashed and Nakagawa, 2004). However, most of the earlier studies consisted of single, 2-D GPR survey lines across faults. Recent work on active faults, (including the San Andreas, Wellington Fault, or Alpine faults), demonstrates that 3-D GPR surveys can provide detailed and accurate subsurface fault zone information, elucidating variations in geometry, offsets of small fault strands, and deformation along the strike of the fault (Gross et al., 2002; Gross et al., 2004; Baldwin et al., 2006; McClymont et al., 2006).

The main objective of this study is to employ 3-D ground-penetrating radar surveying to image fault displacement and assess off-fault deformation associated with the Emigrant Peak fault in central western Nevada, United States. GPR is used to image the main fault, associated fault strands and structures, and stratigraphic features of the faulted alluvial fan. Geological and neotectonic mapping, as well as differential GPS surveys of this site have documented surface offset of alluvial fan surfaces only along the main strand of the Emigrant Peak fault. Faulting produced multiple superimposed fault scarps and uplifted abandoned alluvial fan surfaces. The adjacent alluvial fan surface in the hanging wall of the Emigrant Peak fault lacks any quantifiable surface offset or geomorphic evidence for deformation or faulting. High-resolution geophysical imaging methods can be used to complement neotectonic studies, especially in areas with no measurable surface expression of deformation, and provide important insights for the site selection of time-consuming paleoseismological studies.

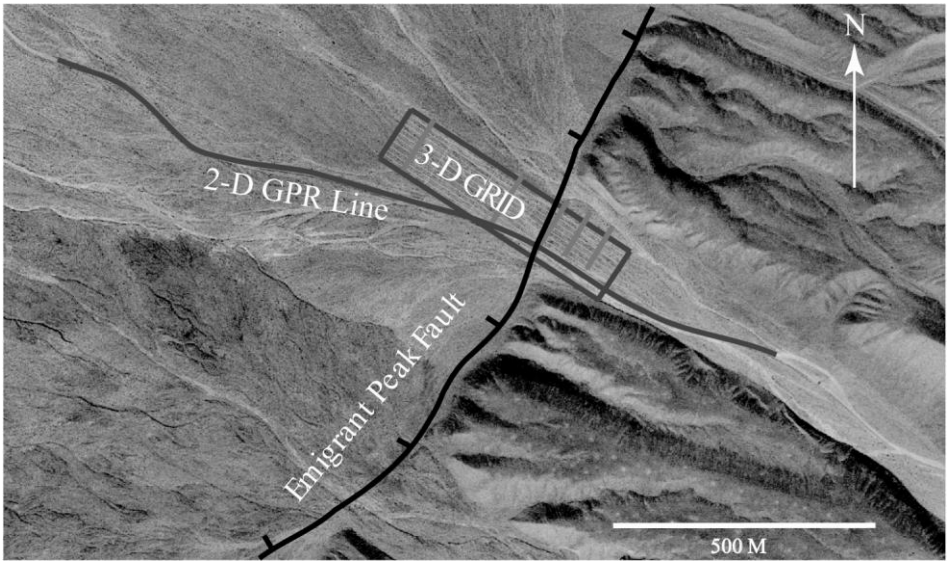

Figure 6. Aerial photograph of the Emigrant Peak fault study area identifying the location of the 3-D grid and 2-D GPR surveys.

Data Acquisition and Processing

GPR Acquisition

Two sets of ground-penetrating radar data were acquired across the Emigrant Peak fault: a high-resolution 3-D survey and a fault-perpendicular, long-baseline 2-D line. The 3-D grid was set up to image both the footwall and hanging wall of the Emigrant Peak fault and architecture of the adjacent associated alluvial fan. The 3-D survey consists of 50 MHz frequency data employing a PulseEKKO PRO GPR system with a 1000 V transmitter, acquired along twenty-four parallel lines with a length of 500 m each and a lateral separation of 5 m. Traces were acquired every 1 m for 501 traces per line, using a sampling interval of 0.8 ns, 32 stacks per trace, and antenna separation of 2 m. The total survey size was 500 m by 115 m. At this site, in order to achieve

complete 3-D subsurface imaging at 50 MHz frequency, a 0.65 m by 0.65 m trace spacing grid is required (Grasmueck et al., 2005). The meter scale lateral extent of features of interest allows for adequate spatial sampling by the 1 m trace spacing employed. However, we recognize that the subsurface was undersampled in the cross-line orientation by the 5 m line spacing. In addition to the 500 m lines, five cross-lines were acquired orthogonally to the in-lines to provide tie points for the 3-D grid. These cross-lines were collected at line positions 50 m, 100 m, 150 m, 250 m, and 450 m with 1 m trace spacing (Fig. 6).

The 2-D line consisted of 25 MHz frequency data acquired with a 1000 V transmitter. The line is 1500 m long, with approximately 500 m of coverage in the footwall and 1000 m in the hanging wall of the active strand of the Emigrant peak fault. Traces were acquired every 1 m for 1501 traces for the line, using a sampling interval of 0.8 ns, 32 stacks per trace, and antenna separation of 4 m. Both GPR datasets used the common-offset method of data collection. Terrain conditions required manual antenna positioning from one trace location to the next (step mode), averaging 2.5 km of radar data collection in a day by a field crew of three persons.

Along with the GPR data lines, differential GPS (DGPS) data were collected to survey the position of each GPR trace location. Accurate spatial positioning is critical for data processing and visualization, mapping of reflectors, and integrating the GPR interpretation with seismic and neotectonic studies

conducted on the Emigrant Peak fault. Elevation changes are approximately 20 m along the 500 m long 3-D survey lines and 55 m along the 1500 m 2-D line.

The DGPS data were also used to create a digital elevation model (DEM) of the central portion of the Emigrant Peak fault (Fig. 7). The DEM clearly highlights the topographic changes associated with faulting along Emigrant Peak fault and reveals the different superimposed fault strands and scarps along the main fault that result from down-to-the-NW dip-slip motion. The DEM also shows the existence of several uplifted and abandoned alluvial fan surfaces in the footwall, the differential erosion and retreat of older fault scarps, and the truncation of these surfaces by several generations of normal faults. Minimum offset of the youngest faulted surface (Q1) and of the surveyed area is 1-2 meters, while minimum offset of oldest surfaces is ~ 35 m (Q3) (Fig. 7) (pers. comm. Schroeder, 2007).

GPR Processing

Different processing sequences were applied to the 3-D and 2-D datasets. Processing the 3-D dataset began with a topographic correction using a ground velocity of 0.13 m/ns obtained from a CMP survey and the elevation data gathered from the DGPS survey. The topographic correction was applied to each line individually. A high-pass frequency "dewow" filter was applied to remove instrumentation noise from the data. The data were converted to SEG-Y format and binned into a 3-D volume. This included renaming parts of the headers into CMP lines, locations, receiver locations, etc. Once the data were binned, AGC

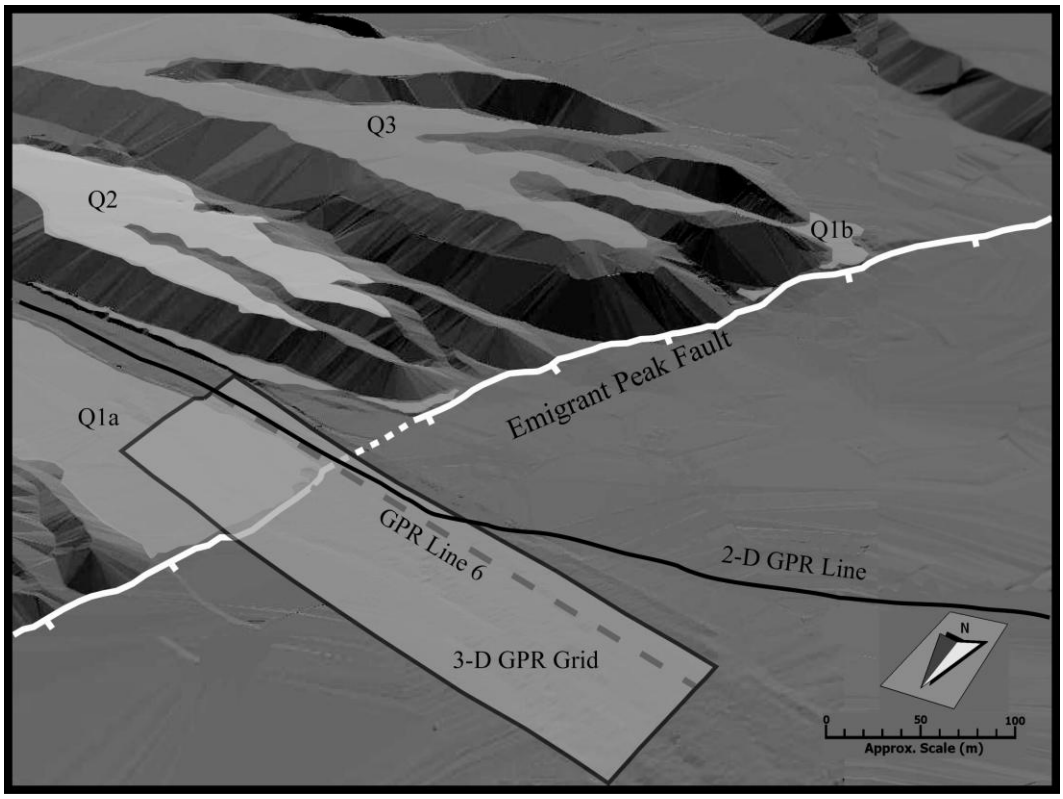

Figure 7. Digital elevation model generated from RTK DGPS survey data, with the location of the Emigrant Peak fault, mapped geomorphic surfaces (Q1, Q2, and Q3), and the location of the 3-D GPR grid and the 2-D GPR line. Geomorphic surfaces from unpublished mapping by J. Schroeder.

amplitude gain and recording delay removal were applied. 2-D migration of the data yielded marginal improvement of the sections due to low-dip angle of the reflectors. 3-D migration resulted in over-migrated data, and it was not applied in the final processing sequence. After processing, the georeferenced data volume was loaded into an interpretation software package.

The 2-D line was processed similarly, including topographic corrections, "dewow" filter and AGC amplitude gain. In addition, a 1000 average trace background subtraction spatial filter was applied to remove horizontal banding

present in the data. A georeferenced line was loaded into the interpretation software and integrated with the 3-D grid.

GPR Imaging Results and Interpretation

Interpretation of the main strand of the Emigrant Peak fault provides the framework for detailed structural and stratigraphic interpretation in the footwall and hanging wall blocks. The three criteria used to identify the main strands of the Emigrant Peak fault and associated structures are: a) reflector discontinuities, b) reflector dip changes, and c) variations in waveform and relative amplitude. In addition to fault identification in individual survey lines, 3-D correlation of faults across multiple parallel lines allowed for a more rigorous structural interpretation and assessment of along-strike-fault geometry variations.

The alluvial fan stratigraphy adjacent to the Emigrant Peak fault is characterized by a high degree of variability both parallel and orthogonal to the GPR survey lines; this reflects the spatially and temporally complex depositional environment of alluvial fans. Interpreting stratigraphic features in the 3-D dataset is difficult due to a) the highly variable depositional and erosional nature of the alluvial fan, and b) the 5 m spacing of the in-lines in the 3-D survey. In light of meter-scale stratigraphic features in the cross-line orientation, the 5 m survey line spacing proved to be too broad to image coherent alluvial fan stratigraphy.

The lower frequency 25 MHz line imaged less stratigraphic detail than the 50 MHz data and proved to be more suitable for larger scale fault interpretation.

The higher resolution 3-D, 50 MHz data allowed mapping alluvial fan stratigraphy and along-strike variations in fault geometries. Using an average velocity of 0.13 m/ns, determined by a CMP survey, the 25 MHz data imaged to an approximate depth of 40 m at 1.3 m of vertical resolution, whereas the 50 MHz data imaged 25 m deep at 0.65 m resolution.

Figure 8 shows a comparison between the 25 MHz, 2-D line and the spatially coincident line 6 of the 3-D, 50 MHz dataset. In the two GPR lines corresponding faults are identified by the same colors. Due to difference in vertical exaggeration between the two sections, however, the same faults appear to have different apparent dip angles. Faults and reflectors were interpreted using a seismic interpretation and visualization software to ensure consistent selection of faults and reflectors between multiple data sets and multiple line interpretations. As an example, figure 8, shows the surficial expression of Emigrant Peak fault (arrows labeled "EP"). The red fault directly beneath the arrows is interpreted as the main fault due its lateral continuity observed in the 3-D volume. However, the near-surface geophysical data clearly illustrates that faulting is more complex and characterized by multiple normal fault strands, while only one single major fault can be inferred from surficial observations. The faults interpreted near the surface expression of Emigrant Peak fault dip at approximately 70° (adjusted for vertical exaggeration) which is in agreement with geologic studies (Reheis and Sawyer, 1997). The faults interpreted away from the main fault have dips that range from 35° to 65°. The changes in dip follow the

observations of Reheis and Sawyer (1997) who noted the shallowing of fault dips towards the west. A number of the NW-dipping faults are characterized by the existence of antithetic faults that intersect at depth forming small graben structures. These grabens are evident in both GPR data sets, but are most clearly identifiable in the 50 MHz data near positions 250 to 300 and 350 to 400 (Fig. 8). In addition, both data sets show normal faulting hundreds of meters away from the main fault; this reveals off-fault deformation not detectable in surface observations and digital elevation models.

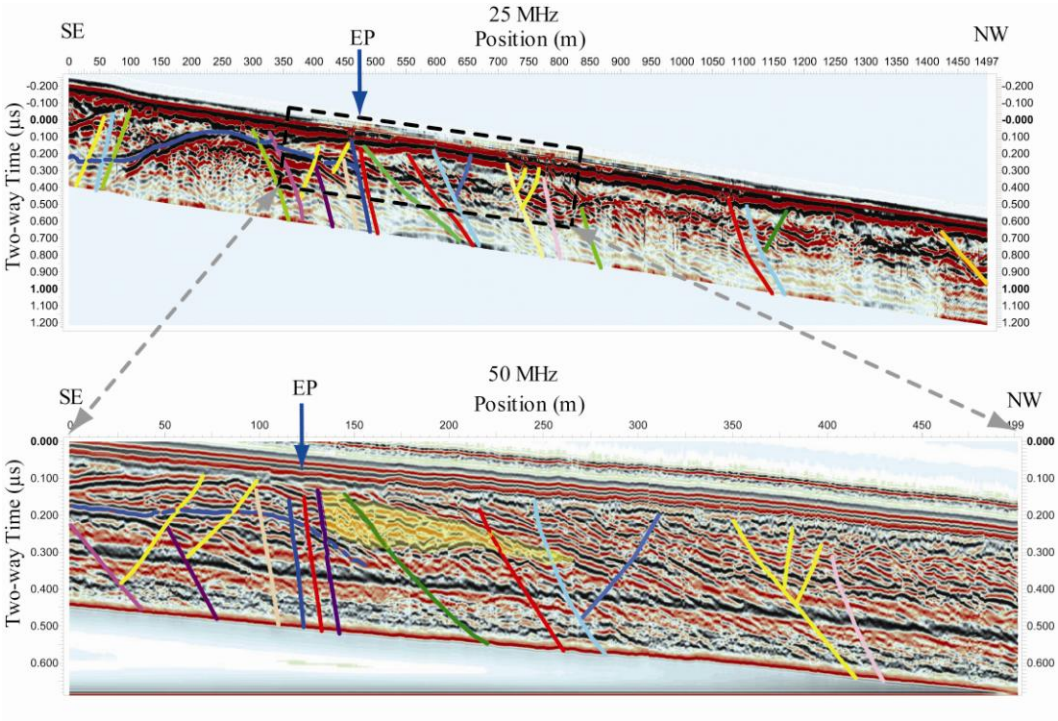

Figure 8. Comparison of coincident 25 MHz (upper) and 50 MHZ (lower) GPR data. The footwall is towards the southeast and the hanging wall towards the northwest. Corresponding fault and horizon interpretations between the two sections are identified by the same colors. GPR amplitudes are represented by black (positive) and red (negative) colors

Line 4 of the 3-D volume (Fig. 9) shows the main fault (red) offsetting the blue horizon by approximately 30 ns of two-way travel time, which corresponds to a vertical offset of 1.95 m. The DEM (Fig. 7) shows a minimum offset of ~1-2 m at the youngest fault scarp, which is in excellent agreement with the GPR subsurface image. The vertical plane in figure 10 is interpreted as the main Emigrant Peak fault, identified as the red fault in two previous figures. This fault is evident across all 24 of the lines that make up the 3-D volume. A prominent marker horizon (blue) is interpretable across approximately one-third of the 3-D dataset (Fig. 10) as well as the 2-D 25 MHz line (Fig. 8). It extends over an area 60 m by 170 m and displays 21 m of relief. We interpret this surface either as the side of an incised channel with the red, upper-portion representing the levee of the channel or alternatively as a depositional lobe of a debris flow, which is the dominant sedimentation mechanism found in Fish Lake Valley alluvial fans (Slate, 1992). The faulted marker horizon (blue) exhibits a clear increase in dip from northeast to southwest, across the fault and in the down-dip direction, providing further evidence that the red fault is the main Emigrant Peak fault.

Moving away from the main fault, reflectors dip basin-ward in both the 25 MHz data and the 50 MHz data (Fig. 8 and 9). These northwest dipping reflectors dominate the data in the hanging wall and are thought to represent progradational patterns of alluvial fan deposition into the basin. Figures 8 and 9 also show wedge-shaped features, highlighted in yellow, within the alluvial fan complex. The wedge feature in figure 8, possibly a colluvial wedge, appears to be truncated

by the main fault and is itself offset by a subsidiary fault (green). In this interpretation, formation of the colluvial wedge would represent multiple faulting

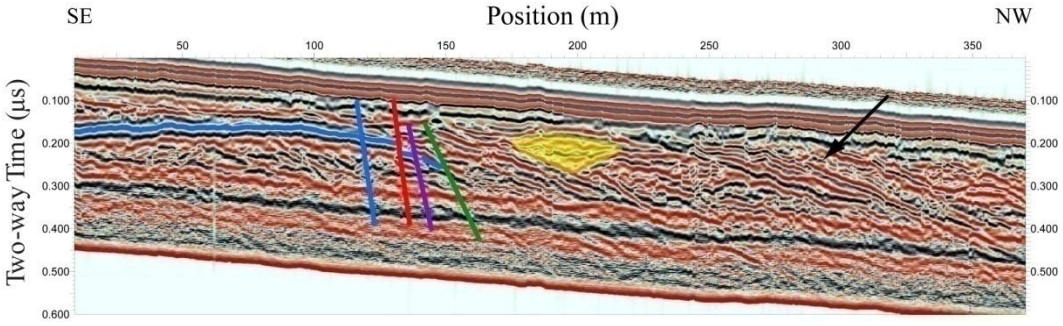

Figure 9. Interpretation of the Emigrant Peak fault along line 4 of the 3-D survey. The blue horizon is offset 30 ns (~1.95 m) by the main fault strand (red). The black arrow points to numerous northwest dipping reflectors which may be related to alluvial fan progradation into the basin.

events with a total displacement of 6.5 m. Alternatively, this wedge-shaped feature could also represent a depositional package related to formation of the alluvial fan, such as an in-filled erosional channel.

In figure 9, a wedge-shaped depositional package is bound on three sides by continuous, strong reflectors. It has a northwest dipping reflector and a southeast dipping reflector as a base and a convex up reflector bounding the top of the package. This feature is 40 m wide at its greatest extent and up to 8 m thick. The feature likely represents channel fill, though colluvial wedge deposition is possible as well. Stratigraphy becomes more difficult to interpret basinward due to the spatially and temporally discontinuous nature of deposition, incision, and erosion of debris flow dominated alluvial fans.

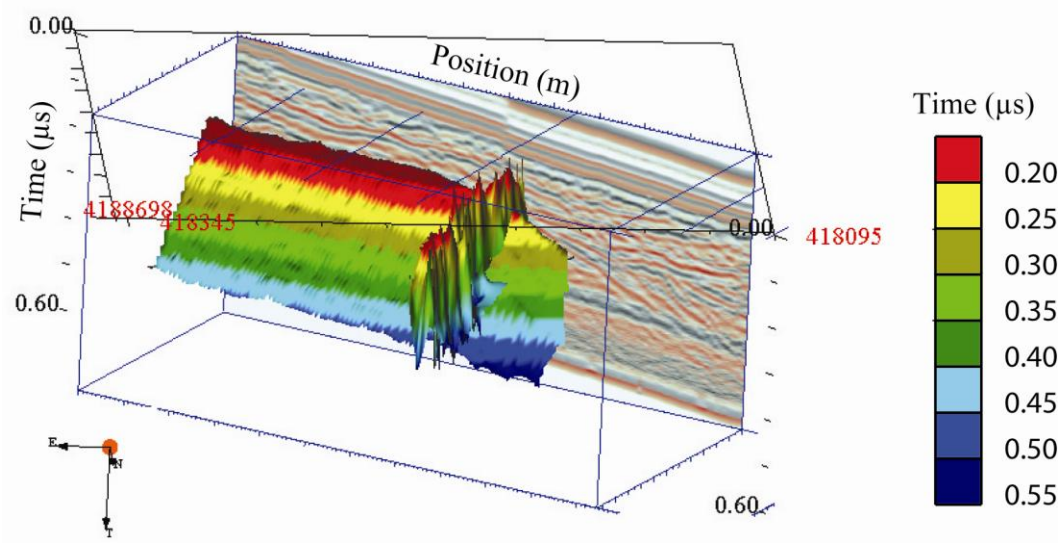

Figure 10. A 3-D view of the main fault interpreted across the entire 3-D survey. A relatively continuous marker horizon (blue) is clearly displaced and tilted due to faulting.

Conclusion

Three-dimensional GPR surveying at the Emigrant Peak Fault in Fish Lake Valley, Nevada, provided high-resolution imaging of an active extensional tectonic setting and the associated alluvial fan. Correlation of faults across multiple parallel lines allowed for detailed structural interpretation and assessment of along-strike-fault geometry variations. Radar data quantified near-surface fault offset at the location of the main fault and revealed considerable off-the-main fault deformation not evident in surface observations, aerial photography, and differential GPS digital elevation models. Diffuse faulting is identified tens to hundreds of meters away from the main fault, both in the footwall and hanging wall blocks imaged by the 3-D and the 2-D GPR lines.

Near the main fault, strata dip to the NW while alluvial fan stratigraphy becomes more complex and discontinuous in the down-dip direction, including possible colluvial wedges, small graben structures, and strata dipping in the opposite direction. Although 3-D GPR surveying yielded detailed subsurface imaging along in-lines, spatial undersampling in the cross-line orientation prevented complete 3-D imaging of meter-scale sedimentary features. Complete subsurface imaging would have required a denser survey grid which would have rendered the acquisition of the data logistically impractical.

GPR imaging of the Emigrant Peak fault is in good agreement with the geologic studies of the region (Reheis and Sawyer, 1997; pers. comm. Schroeder, 2007) and further expands the understanding of processes at an active tectonic setting. Additional 3-D GPR studies along the Emigrant Peak Fault Zone could help assess all deformation along the fault zone by imaging fault geometries and fault interaction with stratigraphy and deposition of alluvial fans.

Integrated SSR and GPR imaging of active faulting

Introduction

The main objective of this study was to image fault displacement and off-fault deformation associated with the Emigrant Peak fault zone (EPFZ) in Fish Lake Valley, Nevada utilizing shallow seismic reflection (SSR) and ground penetrating radar (GPR). The main Emigrant Peak fault is a normal fault accommodating a step-over associated with the regional Death Valley-Furnace Creek-Fish Lake Valley fault system (DV-FC-FLV) (Fig. 11). The detailed objectives included imaging the main fault, associated faults strands and structures, as well as the stratigraphy of the associated alluvial fan and deeper stratigraphic horizons. The main surface expression of faulting is a single fault scarp displaying over 30m of relief across the alluvial fan. Deformation away from the main fault is not evident in any surficial features at the field site.

Shallow seismic reflection (SSR) and ground-penetrating radar (GPR) are geophysical methods that can be used in conjunction with each other to image the subsurface at complementary depths and spatial resolution. SSR can image the upper few hundred meters of the subsurface, while GPR can provide images of the upper tens of meters. SSR images the subsurface with a spatial resolution of several meters, while GPR can image at the meter to sub-meter scale. The combination of the two methods allows for imaging the near-surface at a very high resolution and the ability to extend the interpretation to depths unattainable by other techniques used in active fault studies. Commonly, geologic and

neotectonic mapping, geochronology techniques, GPS studies of strain rates, and paleoseismic trenching studies have been the means by which fault zones have been characterized. The geophysical techniques used here have the potential to allow accurate extrapolation of these characterizations to greater depths than would otherwise be possible.

SSR surveys and GPR surveys have been successfully utilized to image active fault zones in previous studies. Some prior studies have taken advantage of the methods individually (Harris et al., 1998; Baldwin et al., 2006; R. Gross, A. Green et al., 2002; Gross et al., 2004; McClymont et al., 2006), while some have utilized both methods in order to get a more complete image of the subsurface (Pratt et al., 1998; Bano et al., 2002; Rashed and Nakagawa, 2004; Demanet et al., 2001; Chow et al., 2001). Though both methods can be useful individually, their combination provides for more comprehensive geophysical imaging of an active fault zone.

Data Acquisition and Processing

Data Acquisition

The shallow seismic reflection data consisted of two 2-D CMP lines; a 428 m survey perpendicular to, and crossing, the Emigrant Peak fault and a 96 m cross-line recorded on the footwall of the fault. The data was collected with a 144 channel recording system. Receiver groups consisted of a single 28 Hz geophone

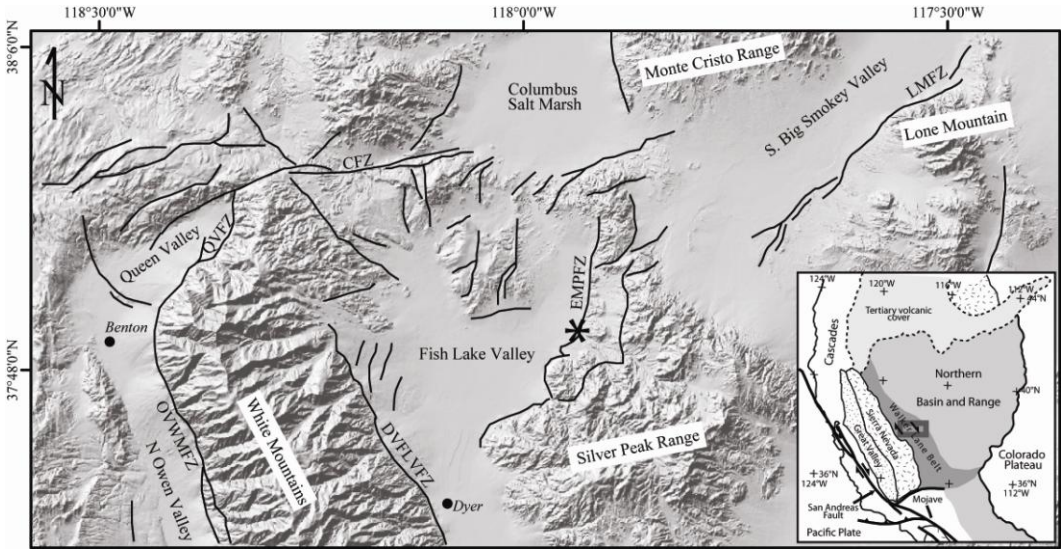

Figure 11. Digital shaded-relief map of west-central Nevada and east-central California, showing major late Cenozoic faults (modified after Oldow 1992, Stockli, et al., 2003) and insert map of Western US tectonic provinces. The shaded box in the insert map outlines the area of the shaded relief map. Map key: OVWMFZ, Owens Valley-White Mountain fault zone; QVFZ, Queen Valley fault zone; CFZ, Coaldale fault zone; DVFLVFZ, Death Valley-Furnace Creek-Fish Lake Valley fault zone; EMPFZ, Emigrant Peak fault zone; LMFZ, Lone Mountain fault zone.

at each station. The geophone spacing was 0.5 m and shot points were located every 1 m. Figure 12 illustrates the survey geometry. Nominal subsurface coverage for the lines was 24 fold, but extra shots were added at the beginning and end of each line to enhance fold at these locations. The seismic source was a modified 30.06 caliber rifle fired with the barrel inserted into a shallow (0.3m) hole at each shot point. The recorded trace length was 1024 ms and the sampling interval was 0.25 ms.

To directly complement the SSR data, GPR data were collected along the same lines as the seismic data. The 2-D GPR data collected along the seismic

lines utilized 25 MHz frequency antenna with a separation of 4m, powered by a 1000 V transmitter. Traces were acquired every 1 m with a sampling interval of 0.8 ns and 32 stacks per trace. The common-offset method of GPR data collection was utilized for both lines.

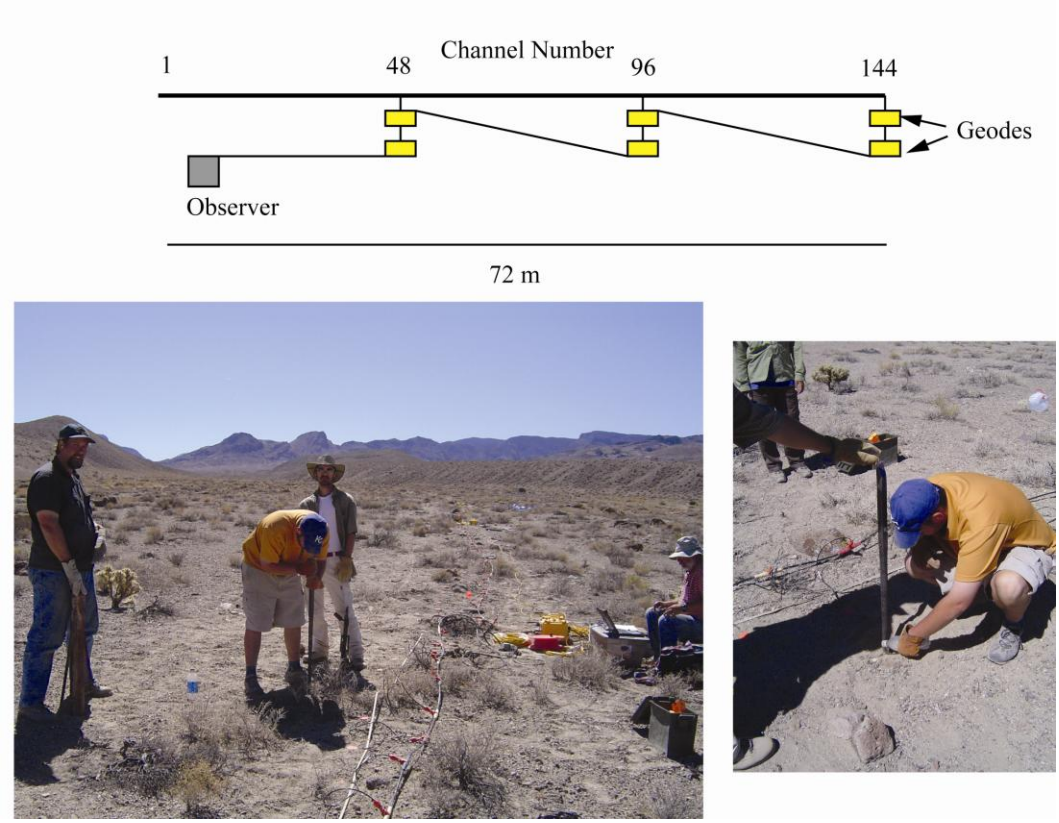

Figure 12. Schematic of the setup for the shallow seismic reflection survey. The yellow boxes represent the Geode seismographs which record 24 channels each. The observer is where the laptop controlling the seismographs is located. The photos illustrate the preparation of shot holes for the rifle source.

Differential GPS (DGPS) was collected to aid in the data processing and to create a digital elevation model (DEM) (Fig. 13). The GPS data was collected in real-time kinematic mode with approximately decimeter accuracy. Elevation changes along the main seismic line were on the order of 16 m, with elevation

decreasing from east to west into the basin. Elevation changes along the cross-line were only about one meter. The DEM (Fig. 13) shows the topographic changes associated with the faulting. The fault scarps resulting from purely dip-slip motion, down to the NW, cut several generations of alluvial fan surfaces. Minimum offset of the youngest faulted surface (Q1) in the region where geophysical data was acquired is 1-2 meters. Minimum offset of the oldest surface (Q3) is as much as 35 m.

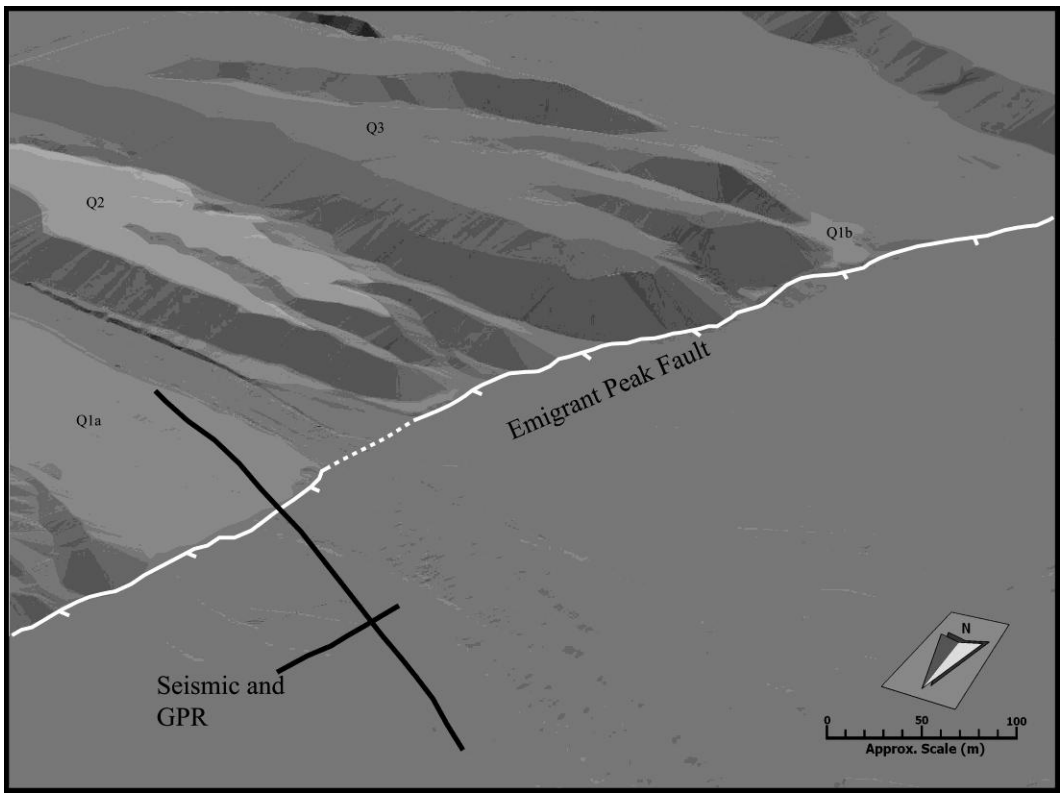

Figure 13. Digital elevation model generated from RTK DGPS survey data, with the location of the Emigrant Peak fault, mapped geomorphic surfaces (Q1, Q2, and Q3), and the location of the SSR and the 2-D GPR lines. Geomorphic surfaces from unpublished mapping by J. Schroeder.

Data Processing

The same data processing flow was used in processing both seismic CMP lines. The flow included field geometry assignment, elevation statics application, and trace editing prior to CMP sorting. After CMP sorting velocity analysis was performed using constant velocity stacks, an NMO correction with stretch muting was applied, an additional early mute was applied, and residual statics corrections were performed. This was followed by an inverse NMO step and a second iteration of velocity analysis. A 20 to 80Hz bandpass filter was then applied to the data. The data were sorted to common offset gathers and a dip moveout correction was applied. The data were then resorted to CMP gathers and stacked. Post stack Kirchoff migration was also applied to the data. The velocity function used in the migration step was a scaled version of the final NMO velocity function. The velocity scaling factor utilized in the final migration was 75%. A spherical divergence correction was applied to enhance data viewing. The last step was to convert the data to depth using a constant velocity of 450 m/s.

The radar data required much less processing than the seismic data. The radar data first had a topographic correction applied utilizing the differential GPS elevations and a ground velocity of 0.13 m/ns derived from a GPR CMP survey. A high-pass 'dewowing' filter was applied to remove low frequency instrumentation noise from the data. This filter did not remove all low frequency noise from the data, however, and a distinct horizontal banding was still present in the data. This banding was buried in the background by signal at the top of the

section, but began to overwhelm the geological signal at greater travel times. To eliminate this banding a moving averaged 'pilot trace' was subtracted from every data trace. This proved more effective than true spatial filtering. To create the pilot trace a sliding window of 95 traces was averaged and the resultant pilot trace was subtracted from the trace in the center of each window. A gain function was then applied to the data to boost the amplitude of deeper events. The final data processing step was depth conversion using a velocity of 0.13 m/ns.

SSR and GPR Imaging Results and Interpretation

The interpretation of the SSR, GPR and GPS datasets was performed in an integrated manner. The location of the main surficial fault scarp was determined from the DGPS data. This location was then transferred to both the GPR section and the seismic section to ensure correspondence between the two data sets. All structures were also interpreted on both sections to retain this continuity. A fault was not interpreted in the seismic if it was not visible in the GPR data and vice-versa. The faults were identified in the sections by: a) reflector discontinuities, b) abrupt reflector dip change, and c) variations in waveform and relative amplitude.

Figure 14 shows both the GPR and the SSR sections that are perpendicular to the strike of the main Emigrant Peak fault. The faults in both data sets are color-coordinated to match between the sections. The GPR image corresponds approximately to the upper 40 m, or 0.20 seconds, of the SSR section. The sections show northwest dipping faults with 2 southeast dipping antithetic faults.

The vertical resolution of the 25MHz GPR section is slightly more than 1 m. The main fault is represented by the red fault in both sections located at approximately position 150. This location represents the surficial fault scarp at the field site. The GPR data may not illustrate the amount of offset along the faults that the SSR data shows. The two different methods respond to different physical properties and this may cause the differences present in the two sections. The GPR is also imaging much younger sediment than the SSR.

The fault dips are very similar to fault dips that have been measured in field studies. Reheis and Sawyer (1997) measured dips ranging from 45º to 70º which correspond well with those observed on the GPR and SSR sections. The faults in the GPR section have slightly shallower dips than the corresponding faults in the SSR data. The faults range from approximately 45º to 80º, though the main fault dipping at 80º shallows to 65º near the bottom of the section.

The GPR and SSR sections also show stratigraphic features that give insight into alluvial fan deposition and possible deposition related to faulting events. The GPR shows a number of reflectors that dip towards the northwest, or basinward, that may represent progradation of the alluvial fan. There are two distinctive packages that can be interpreted from the GPR section. The base of each package is illustrated in figure 15. Similar features can be seen in the SSR section as well. The stratigraphy is very complex and difficult to accurately interpret. The amount of movement on the faults really hinders the stratigraphic interpretations of the section. With the amount of fault movement, the best

images of field site stratigraphy may be obtained from the cross-line GPR and SSR data.

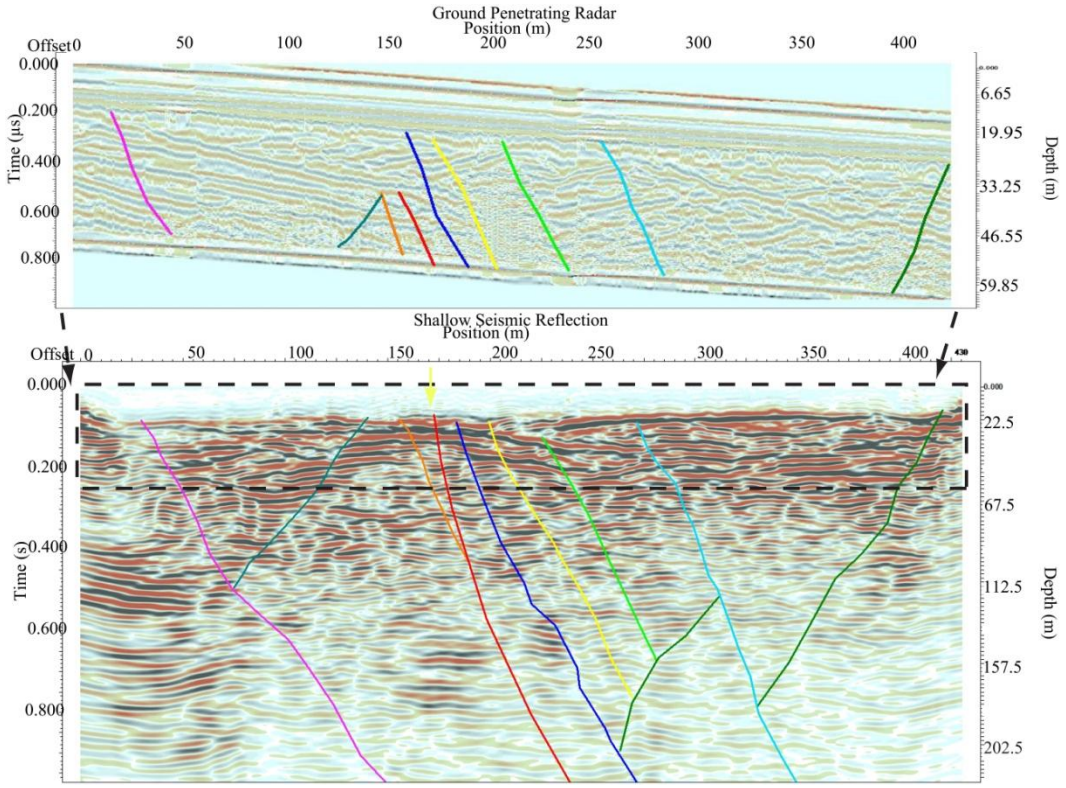

Figure 14. Comparison of coincident 25 MHz GPR and SSR. The faults are color coded to correlate between the GPR and SSR sections. The black, dashed box in the seismic data represents the area that the GPR data overlaps with the SSR data. The yellow arrow represents the surface expression of the Emigrant Peak fault. The sections have both time and depth scales, though the time scales are not the same for GPR (µs) and SSR (s).

The offset that is exhibited in the sections along with the complex stratigraphy associated with alluvial fans makes stratigraphic interpretations difficult. The limited lateral extent of both the GPR and SSR data limited the ability to actually distinguish individual flow events within the alluvial fan. This

being the case, stratigraphic interpretations were not used to determine the overall alluvial fan architecture, but were used to estimate offsets associated with faulting and identify individual stratigraphic features.

Figure 16 shows the GPR and SSR cross-lines. The GPR data does not have laterally continuous reflectors across the section but exhibits reflectors dipping towards the northeast and southwest. Possible channel features can be interpreted in the data. The SSR cross-line data (Fig. 17) shows complex depositional features towards the top and middle of the section and gets less complex with depth. Various channel features associated with alluvial fan deposition can be interpreted from the SSR section.

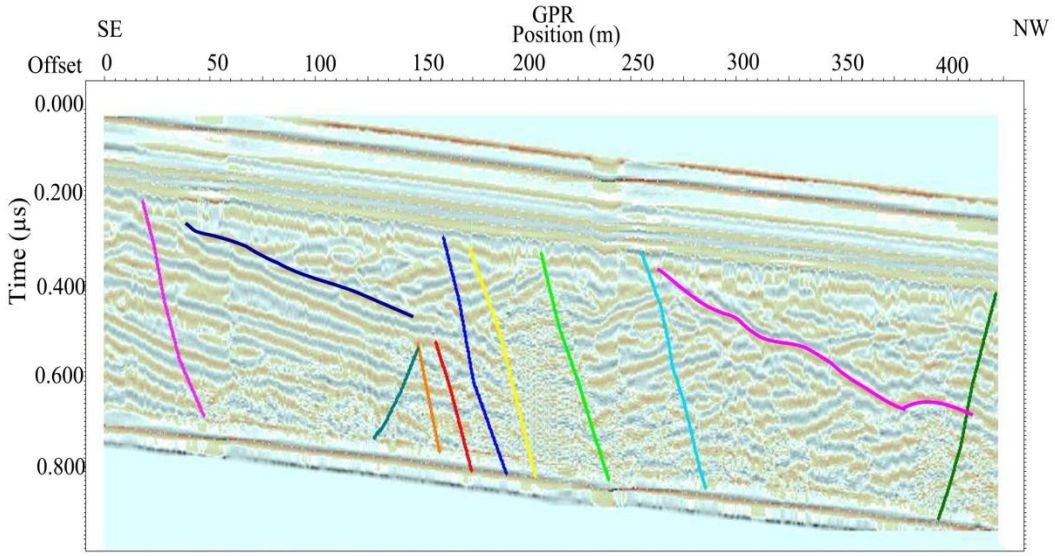

Figure 15. Interpreted GPR data. The interpreted reflectors illustrate the basinward dip of the alluvial fan stratigraphy.

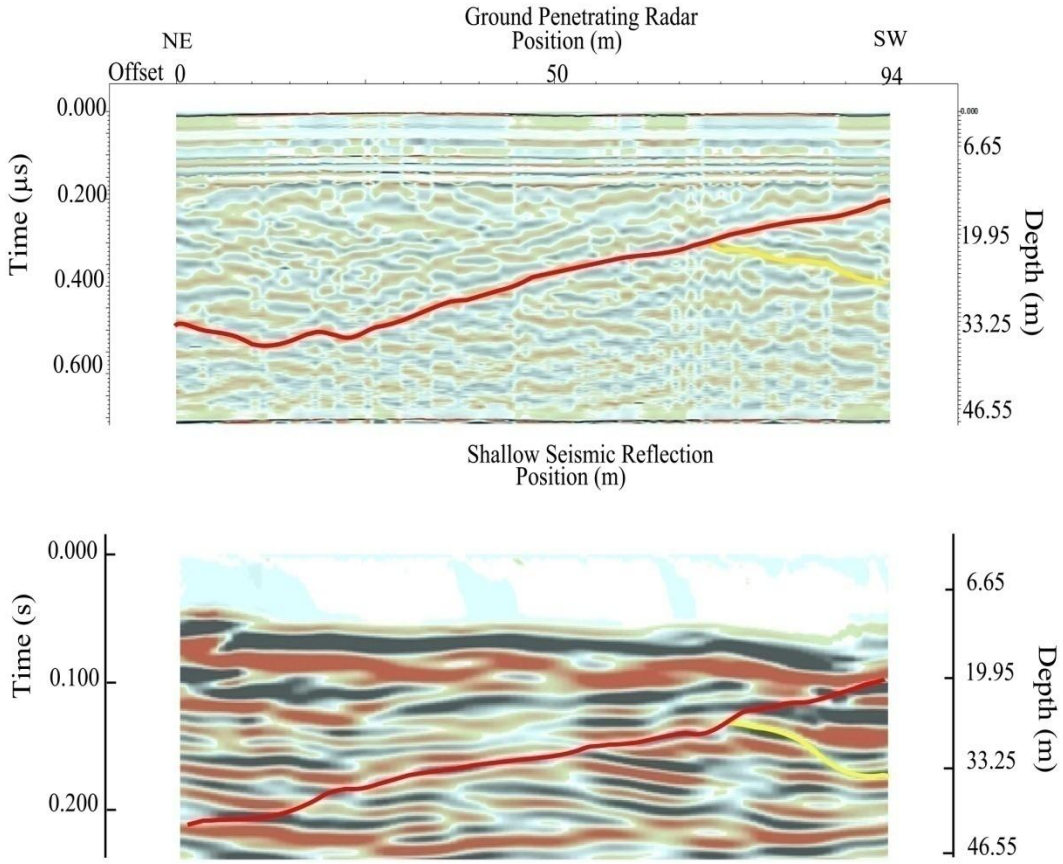

Figure 16. Comparison of the GPR and SSR cross-lines showing data to the same depth. The stratigraphic interpretations illustrate the channel-like nature of alluvial fan deposition in the region. The sections have both time and depth scales, though the time scales are not the same for GPR (µs) and SSR (s).

Conclusions

The combination of ground-penetrating radar and shallow seismic reflection techniques allow for imaging of the subsurface in this portion of the Fish Lake Valley, from the ground surface to a depth of approximately 225 m. Using surface information extrapolated into subsurface images generated by the geophysical techniques is very important when trying to characterize the structures and stratigraphy in the subsurface. The data shows a cluster of faults

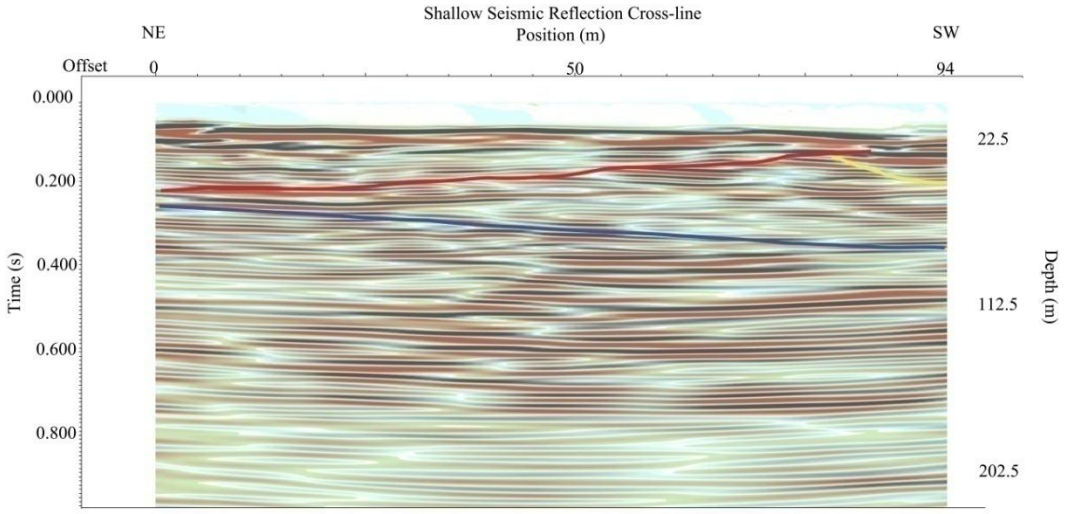

Figure 17. SSR cross-line data illustrating the channel-like nature of alluvial fan deposition.

around the main Emigrant Peak fault that are not observable at the surface. There are also faults 100 m away from the main fault in both the footwall and hanging wall of the Emigrant Peak fault. The dips of the interpreted faults also fall within the range measured in previous geological field studies. Some stratigraphic packages and geometries are interpretable, but do not provide highly detailed stratigraphic information. The data sets documented here should help reconcile geologic displacement and slip-rates with rates from geodetic studies by providing information about off-fault deformation. Using both GPR and SSR provides a means of extrapolating surficial data to depths over 200 m for a more complete characterization of the Emigrant Peak fault zone.

Summary

The objective of this project is to use ground-penetrating radar (GPR) and shallow seismic reflection (SSR) techniques to better characterize the Emigrant Peak fault zone in Fish Lake Valley, Nevada. Some of the information sought using these geophysical techniques included the feasibility of imaging the associated alluvial fan, the stratigraphy in the alluvial fan, the location of the fault at depth, and the structures associated with the main fault (unmapped fault strands, other deformational features, colluvial wedge deposition, and stratigraphic changes associated with faulting). The data presented has illustrated that the Emigrant Peak fault can be imaged with both GPR and SSR. The data shows the main fault as well as faults located away from the main scarp in both the footwall and hanging wall. The faults away from the main scarp do not exhibit any discernable surficial features. This result is very important when trying to compare the measured geologic rates to measured geodetic rates.

Three-dimensional GPR imaging is very important when trying to completely characterize the fault zone. Determining the areal extent of fault strands and associated structures allows for better estimates of total fault zone deformation. Tracing fault strands throughout the data set offers better understanding of the extent of faulting around the main fault. The ability to locate faults in the subsurface that may only exist for a few tens of meters is still very important when trying to compare geologic and geodetic rates. Discrepancies in the two rates are generally due to unmapped faults that take up strain. A few

faults clustered around the main fault, as seen in the 3-D GPR data, could each take up a portion of the overall strain budget and then the main fault would not present the same geodetic and geologic slip rates. Geologic rates provide information about present day processes. The difference could be related to the amount of time the measurements are taken compared to the extent of the geologic record. Perhaps there are short-term cycles that cannot be taken into account in the geologic record. Perhaps the actual tectonics of the area is changing. Subsurface geophysical imaging can help resolve some of these questions and offer better characterization of fault zones. Better understanding of fault zones also provides for better seismic hazard assessments.

Three-dimensional GPR imaging was used to investigate the top 25-40 m of the subsurface. The 3-D data illustrates that faults are interpretable 100 m away from the main fault, and surficial fault scarp in the footwall and 250 m in the hanging towards the basin. Due to the longer length of the 2-D GPR line faults are interpretable up to 400 m away in the footwall and 650 m in the hanging wall. The information about the Emigrant Peak fault gained from the surveys corresponds very well with neotectonic data gathered at the surface. The main fault associated with the fault scarp is identifiable in the subsurface at the expected location. The data also shows offset in the subsurface that corresponds to the 1-2 m scarp at the surface. The dip angles of the interpreted faults are also in agreement to those found in a neotectonic study. The faults interpreted near the surface expression of Emigrant Peak fault dip at approximately 70° which

coincides with geologic data collected for Emigrant Peak fault (Reheis & Sawyer, 1997). The faults interpreted away from the main fault have dips that range from 35° to 65°.

The stratigraphy of the alluvial fan is difficult to interpret due to the limited continuity of reflections but it was useful in helping to determine fault offsets. Offset reflectors 5-10 m below the surface showed comparable displacement to the 1-2 m scarp that is present at the surface. The 3-D data allows for interpretations along the imaged length of a fault. Three faults, including the main fault strand, were interpreted across the entire breadth of the 3-D GPR survey. Several other faults were interpreted throughout the 3-D data set. Not all of the faults were able to be interpreted across the entire 3-D volume. Some of the faults merge into others and some just are no longer interpretable.

The interpretation of the SSR and 2-D GPR data presents different problems and benefits than the 3-D GPR dataset. The main benefit for the SSR and accompanying GPR is the improved depth of investigation. One of the major drawbacks is the loss in vertical resolution when compared to the 50 MHz GPR. The loss in resolution though, is only significant when interpretations of stratigraphy are made. The seismic and accompanying GPR is limited in its interpretation because the data consists of single 2-D lines with a cross-line. The GPR images from the surface a depth of approximately 40 m. The SSR data images the subsurface from depths of approximately 20 m to 230 m. The two techniques use different physical properties to create images of the subsurface, so

while the data may present similar images it may not be possible to correlate surfaces between the GPR and SSR. Important questions such as, what is the geometry at depth, is the fault listric at depth or does it remain relatively straight, or do shallow faults merge at depth, may be able to be answered. The SSR and lower frequency GPR are employed to try to answer these questions.

The GPR imaged approximately the upper 40 m, or 0.20 seconds, of the SSR section. The sections show northwest dipping faults with two antithetic faults dipping towards the southeast. Numerous faults are observed near the location of the main fault. The fault dips are very similar to fault dips that have been measured in field studies. Reheis and Sawyer (1997), measured dips ranging from 45º to 70º, which corresponds well with the data gathered from the GPR and SSR sections. The faults in the GPR section have slightly shallower dips than the corresponding faults in the SSR data. The fault dip angles range from approximately 45º to 80º, though the main fault dipping at ~80º shallows to ~65º near the bottom of the section.

One of the advantages that the SSR section can provide is the ability to measure offset by matching up reflectors along the faults. The potential amount of offset gathered from the SSR exercise of correlating reflectors across the faults ranged from approximately 20 m to 80 m. The average amount of displacement along the faults is ~41 m. The calculated offsets combine to show approximately 370 m of possible displacement along all of the faults. Offset numbers for the Emigrant Peak fault range from 125 m to 735 m and 370 m falls within the

acceptable range for the fault zone (Reheis & Sawyer, 1997). The exercise of trying to identify offset among a number of faults is a very important preliminary result, indicating the strain is distributed among a number of faults, not a single fault. This data can be used as a starting point to reconcile differences between measured geologic rates and geodetic rates. More comprehensive seismic data and well data would have to be used to make the estimations of offset viable.

The GPR and SSR sections also show stratigraphic features that give insight into alluvial fan deposition and possible deposition related to faulting events. The GPR shows a number of reflectors that dip towards the northwest, or basinward, that may represent progradation of the alluvial fan. There are two distinctive packages that can be interpreted from the GPR section. Similar features can be seen in the SSR section as well. The stratigraphy is very complex and difficult to interpret accurately. The amount of movement on the faults hinders the stratigraphic interpretations of the section. With the amount of fault movement, the best images of field site stratigraphy may be obtained from the cross-line GPR and SSR data.

The GPR cross-line data does not have many continuous reflectors across the section but does have reflectors dipping towards the northeast and southwest. It looks like possible channel features can be picked out of the data. The SSR cross-line data shows complex depositional features towards the top and middle of the section and gets less complex with depth, which could be due to an imaging

problem and not necessarily a geologic one. Various channel features associated with alluvial fan deposition can be interpreted from the SSR section.

Recommendations/Future Work

Recommendations

These recommendations concern areas where improvements can be made in data collection, processing, and interpretation. The limiting factor for the amount of seismic data that could be collected was the time required to prepare shot holes for the rifle source. This was the most laborious and time-consuming task associated with collecting the data. If future surveys were conducted in the same way and in a similar environment, it would be important to look at ways to limit the time needed to pre-punch the firing holes. Perhaps the use of an auger or a surface firing system analogous to the Betsy Seisgun could expedite the deployment of the rifle source.

A problem that arose during processing, but related to data acquisition, is associating the GPS data with the geophysical survey locations. GPS data was not taken at every specific data collection location. This adds complexity and more work to combining the geophysical data with the GPS data. Extra calculations have to be made to the GPS data in a spreadsheet to create topographic profiles and files used to geospatially orient the data in the interpretation software. If the GPS data could be taken at every point it would make steps in processing and interpretation much easier. The calculations also add unnecessary error to the GPS readings. Having 300 GPS points for a 500-point survey makes it difficult to be sure about which GPS points correspond to the correct GPR or SSR points.

GPR cross-line spacing needs to equal the 1 m trace spacing in the inline direction in order to be able to use cross-line interpretations. Creating a 3-D volume of GPR in-lines, spaced 5 m apart provided insufficient cross-line spatial resolution for interpretation purposes. Creating a GPR grid with 1 m trace spacing in both the x- and y-directions is necessary for complete interpretation of the data. The cross-line resolution greatly hindered the stratigraphic interpretations in the 3-D GPR data.

Future Work

The first aspect of future wok that should be addressed is expanding the area of GPR and seismic coverage. Ideally, the 3-D GPR data would be complimented by a 3-D SSR survey. The seismic data and 25 MHz GPR overlapped in depth by 20 m, which was half of the GPR section. The 50 MHz data imaged to a depth of approximately 20 m, so it should be feasible that 50 MHz GPR could be used in conjunction with the SSR. 50 MHz GPR has higher resolution than the 25 MHz GPR which allows for better interpretations of stratigraphy which can help with structural interpretations.

In addition of expanding the SSR survey into a 3-D grid, expanding the grid itself is also important work than can be pursued. Imaging more of the fault zone would naturally help us to understand how the fault changes along its length. How displacement changes along the length, the nature of deformational structures, and the interaction of structures with the depositional environment are

all issues that an expanded data set would help to address. Not only can the surveys be expanded along the length of the fault, but they should be expanded further into the footwall and hanging wall as well. Gathering data further into the basin would allow a more complete analysis of how far faulting extends into the basin. The data we have collected already shows that the faulting takes place several 10s to 100s of m away from the main fault into the basin and is not apparent at the surface. Identifying these faults is very important in areas such as seismic hazard assessment and trying to match geologic and geodetic rates in the fault zones.

An important aspect of future work that must be accomplished is applying these techniques at other sites. For example, similar, but very preliminary work has been done in Queen Valley, NV, though the data has yet to be thoroughly analyzed. Active faults with active alluvial fan sedimentation can be found throughout the world. The SSR and GPR techniques presented here are another tool that can be used to add data to help solve questions about fault zones. The techniques can be used virtually anywhere with modifications needed only for the seismic data collection portion. With the technique being so versatile, it should become common procedure to help characterize active fault zones.

References

Argus, D., Gordon, R., 1991. No-net-rotation model of current plate velocities incorporating plate motion model NUVEL-1. *Geophysical Research Letters , 18* (11), 2039-2042.

Atwater, T., 1970. Implications of Plate Tectonics for the Cenozoic Tectonic Evolution of Western North America. *Geological Society of America Bulletin , 81*, 3513-3536.

Baldwin, J., Witter, R., Vaughn, J., Harris, J., Sexton, J., Lake, M., Forman, S.L., Barron, A.D., 2006. Geological Characterization of the Idalia Hill Fault Zone and Its Structural Association with the Commerce Geophysical Lineament, Idalia, Missouri. *Bulletin of the Seismological Society of America , 96* (6), 2281-2303.

Bano, M., Edel, J., Herquel, G., 2001-2002 EPGS class, 2002. Geophysical Investigation of a recent shallow fault. *The Leading Edge* , 648-650.

Beaty, C., 1963. Origin of alluvial fans, White Mountains, California and Nevada. *Annals of the Association of American Geographers , 53* (4), 516.

Bennett, R., Davis, J., Wernicke, B., 1999. Present-day pattern of Cordilleran deformation in the wester United States. *Geology , 27* (4), 371-374.

Blair, T., McPherson, J., 1992. The Trollheim alluvial fan and facies model revisited. *Geological Society of America Bulletin , 104*, 762-769.

Bradley, D., Stocklie, D., Lee, J. (in review). Kinematic evolution of the Coaldale Fault and implications for the Mina Deflection, Nevada. *Geological Society of America Bulletin* .

Bull, W., 1977. The alluvial-fan environment. *Progress in Physical Geography , 1* (2), 222-270.

Chow, J., Angelier, J., Hua, J.-J., Lee, J.-C., Sun, R., 2001. Paleoseismic event and active faulting: from ground penetrating radar and high-resolution seismic reflection profiles across the Chihshang Fault, eastern Taiwan. *Tectonophysics , 333*, 241-259.

Davis, J., Annan, A., 1989. Ground-Penetrating Radar for High-Resolution Mapping of Soil and Rock Stratigraphy. *Geophysical Prospecting , 37*, 531-551.

Demanet, D., Renardy, F., Vanneste, K., Jongmans, D., Camelbeeck, T., Meghraoui, M., 2001. The use of geophysical prospecting for imaging active faults in the Roer Graben, Belgium. *Geophysics , 66* (1), 78-89.

Demets, C., Dixon, T., 1999. New kinematic models for Pacific-North America motion from 3 Ma to present; I, Evidence for steady motion and biases in the NUVEL-1A model . *Geophysical Research Letters , 26*, 1921-1924.

Diamond, D., Ingersoll, R., 2002. Structural and Sedimentologic Evolution of a Miocene Supradetachment Basin, Silver Peak Range and Adjacent Areas, West-Central Nevada. *Internation Geology Review , 44*, 588-623.

Ekes, C., Hickin, E., 2001. Ground penetrating radar facies of the paraglacial Cheekye Fan, southwestern British Columbia, Canada. *Sedimentary Geology , 143*, 199-217.

Grasmueck, M., Weger, R., Horstmeyer, H., 2005. Full-resolution 3D GPR imaging. *Geophysics , 70* (1), K12-K19.

Gross, R., Green, A., Horstmeyer, H., 2004. Location and geometry of the Wellington Fault (New Zealand) defined by detailed three-dimensional georadar data. *Journal of Geophysical Research , 109* (B05401), 1-14.

Gross, R., Green, A., Holliger, K., Horstmeyer, H., Baldwin, J., 2002. Shallow geometry and displacements on the San Andreas Fault near Point Arena based on trenching and 3-D georadar surveying. *Geophysical Research Letters , 29* (20), 34-1-34-4.

Harris, J., Berman, S., Beard, W., Street, R., Cox, R., 1998. Shallow seismic reflection investigations of neotectonic activity in the Lower Mississippi Valley. *SEG Expanded Abstracts* , 1-4.

Hooke, R., 1967. Processes on Arid-Region Alluvial Fans. *Journal of Geology , 75*, 438-460.

Keller, E., Pinter, N., 2002. *Active Tectonics: Earthquakes, Uplift, and Landscape.* Prentice Hall.

Lee, J., Spencer, J., Owen, L., 2001. Holocene slip rates along the Owens Valley fault, California: Implications for the recent evolution of the Eastern California Shear Zone. *Geology , 29* (9), 819-822.

McCalpin, J., 1996. Paleoseismology in Extensional Tectonic Environments. In J. McCalpin (Ed.), *Paleoseismology* (pp. 85-146). Academic Press.

McClymont, A., Streich, R., Heincke, B., Green, A., 2006, June 19-22. Visualization of active4 faulting using 3-D GPR data recorded across the Alpine Fault, New Zealand. *11th International Conference on Ground Penetrating Radar* , 1-5.

Miller, M., Johnson, D., Dixon, T., Dokka, R., 2001. Refined kinematics of the eastern California shear zone from GPS observations, 1993-1998. *Journal of Geophysical Research-Solid Earth , 106*, 2245-2263.

Miller, M., Webb, F., Townsend, D., Golombek, M., Dokka, R., 1993. Regional coseismic deformation from the June 28, 1992, Landers, California, earthquake-results from the Mojave GPS network. *Geology , 21*, 868-872.

Miller, R., Steeples, D., 1996. *Evaluation of Fault Scarp at Harlan County Lake, Harlan County, Nebraska using High Resolution Seismic Reflection Surveying.* Lawrence, KS: Kansas Geological Survey.

Mills, H., Speece, M., 1997. Ground-Penetrating Radar exploration of Alluvial Fans in the Southern Blue Ridge Province, North Carolina. *Environmental & Engineering Geoscience , 3* (4), 487-499.

Nelson, A., 1992. Lithofacies Analysis of Colluvial Sediments- an Aid in Interpreting the Recent History of Quaternary Normal Faults in the Basin and Range Province, Western United States. *Journal of Sedimentary Petrology , 62* (4), 607-621.

Oldow, J., 2003. Active transtensional boundary zone between the western Great Basin and Sierra Nevada block, western U.S. Cordillera. *Gewology , 31* (12), 1033-1036.

Oldow, J., 1992. Late Cenozoic displacement partitioning in the northwestern Great Basin. (S. Craig, Ed.) *Structure, tectonics, and mineralization of the Walker Lane, Walker Lane Symposium Proceedings*, 17-52.

Oldow, J., Aiken, C., Hare, J., Ferguson, J., Hardyman, R., 2001. Active displacement transfer and differential block motion within the central Walker Lane, western Great Basin. *Geology , 29* (1), 19-22.

Oldow, J., Kohler, G., Donelick, R., 1994. Late Cenozoic extensional transfer in the Walker Lane strike-slip belt, Nevada. *Geology , 22*, 637-640.

Petronis, M., 2005. Heterogeneous Block Rotations in Mina Deflection of the Central Walker Lane, West Central Nevada. *Geological Society of America Abstracts with Programs , 37* (7), 70.

Pratt, T., Dolan, J., Odum, J., Stephenson, W., Williams, R., Templeton, M., 1998. Multiscale seismic imaging of active fault zones for hazard assessment: A case study of the Santa Monica fault zone, Los Angeles, California. *Geophysics , 63* (2), 479-489.

Rashed, M., Nakagawa, K., 2004. High-resolution shallow seismic and ground penetrating radar investigations revealing the evolution of the Uemachi Fault system, Osaka, Japan. *The Island Arc , 13*, 144-156.

Reheis, M., Dixon, T., 1996. Kinematics of the Eastern California shear zone: Evidence for slip transfer from Owens and Saline Valley fault zones to Fish Lake Valley fault zone. *Geology , 24* (4), 339-342.

Reheis, M., Sawyer, T., 1997. Late Cenozoic history and slip rates of the Fish Lake Valley, Emigrant Peak, and Deep Springs fault zones, Nevada and California. *Geological Society of America Bulletin , 109*, 280-299.

Reheis, M., Sarna-Wojcicki, A., Meyer, C., McKee, E., Slate, J., Burbank, D., Sawyer, T.L., Pendall, E.G., 1991. *Late Cenozoic Stratigraphy and Tectonics of Fish Lake Valley, Nevada and California: Road Log and Contributions to the Field Trip Guidebook, 1991 Pacific Cell, Freinds of*

the Pleistocene. Open-File Report 91-290, U.S. Department of the Interior Geological Survey.

Reheis, M., Slate, J., Sarna-Wojcicki, A., Meyer, C., 1993. A late Pliocene to middle Pleistocene pluvial lake in Fish Lake Valley, Nevada and California. *Geological Society of America Bulletin , 105*, 953-967.

Reheis, M., Slate, J., Throckmorton, C., McGeehin, J., Sarna-Wojcicki, A., Dengler, L., 1996. Late Quaternary sedimentation on the Leidy Creek fan, Nevada-California: geomorphic responses to climate change. *Basin Research , 12*, 279-299.

Savage, J., Lisowski, M., Prescott, W., 1990. An apparent shear zone trending north-northwest across the Mojave Desert into Owens Valley. *Geophysical Research Letters , 17*, 2113-2116.

Sawyer, T., 1990. Quaternary geology and neotectonic activity along the Fish Lake Valley fault zone, Nevada and California. *Thesis* . University of Nevada, Reno.

Sexton, J., Jones, P., 1986. Evidence for recurrent faulting in the New Madrid seismic zone from Mini-Sosie high-resolution reflection data. *Geophysics , 51* (9), 1760-1788.

Slate, J., 1992. Quaternary Stratigraphy, Geomorphology and Geochronology of Alluvial Fans, Fish Lake Valley, Nevada-California. *Dissertation* . University of Colorado.

Stockli, D., Dumitru, T., McWilliams, M., Farley, K., 2003. Cenozoic tectonic evolution of the White Mountains, California and Nevada. *GSA Bulletin , 115* (7), 788-816.

Udphuay, S., Wood, S., Liberty, L., 2004. Outcrop-scale imaging of lacustrine delta sediments using ground penetrating radar and seismic methods. *SEG Int'l Exposition and 74th Annual Meeting* , 4.

Wesnousky, S., 2005. Active faulting in the Walker Lane. *Tectonics , 24* (TC3009), 1-35.

Wesnousky, S., 2005. The San Andreas and Walker Lane fault systems, western North America: transpression, transtension, cumulative slip and the structural evolution of a major transform plate boundary. *Journal of Structural Geology , 27*, 1505-1512.

Williams, R., Simpson, R., Jachens, R., Stephenson, W., Odum, J., Ponce, D., 2005. Seismic relfection evidence for a northeast-dipping Hayward fault near Fremont, California: Implications for seismic hazard. *Geophysical Research Letters , 32* (L13301), 1-4.

Woolery, E., Street, R., Wang, Z., Harris, J., McIntyre, J., 1999. Neotectonic Structure in the Central New Madrid Seismic Zone: Evidence from Multimode Seismic-reflection Data. *Seismological Research Letters , 70* (5), 554-576.

Appendix

GPR Processing Procedure for 3-D data

1. The de-wow filter was applied in GPR Ekko View software using default parameters.
2. The GPS data was interpolated to include a reading for every trace location for the GPR data.
3. The elevation correction was applied to each line in the Ekko View software using a velocity of .133 m/ns. A topography file was created using the GPS data and then applied using the 0.133 m/ns velocity.
4. All the processed data files and related headers that make up the 3-D volume are copied into a single file folder.
5. The I/O Utility in SPW is used to convert the Sensors and Software data into the SPW format. The *data format* button was used to format and the input file was assigned as first GPR line. The file type used is *Sensors & Software.* The box for the input of multiple files was checked. The output type should be SPW format and then volume was given a name. This step put all of the GPR lines into a single SPW file.
6. The SPW Flow software was used to adjust the GPR headers to comply with the SPW software. 6 *Trace Header Column Math* modules were used in succession with the following parameters with the *equal to A* button selected:

Output Header	Header Field A
CMP Line	Field File
CMP Location	Channel Number
Source Line	Field File
Source Location	Channel Number
Receiver Line	Field File
Receiver Location	Channel Number

7. The recording delay removal was done by using *Apply Static Shifts* using bulk shift of -87.080.
8. The *Automatic Gain Control* with a start of 0.00 and window of 29.6 was used to enhance the image by boosting the amplitude of reflectors at depth.
9. *Phase Shift Migration* was applied in the inline direction using a constant velocity of 133 m/s and then applied in the same way in the cross-line direction.
10. Further processes can be applied as well, including filtering the data.

GPR Processing Procedure for 2-D lines

1. The de-wow filter was applied in GPR Ekko View software using default parameters.

2. The GPS data was interpolated to include a reading for every trace location for the GPR data.
3. The elevation correction was applied to each line in the Ekko View software using a velocity of .133 m/ns. A topography file was created using the GPS data and then applied using the 0.133 m/ns velocity.
4. The *background subtraction filter* was applied in Ekko View to remove horizontal banding, an artifact of data collection, from the data.
5. If necessary, filters can be applied to enhance the data.

Seismic Data Processing

1. The data was reformatted from SEG-2 files to SPW files, which was done in the SPW I/O Utility.
2. The data for this study used three steps to apply the acquisition geometries to the seismic file headers. The data was separated into three different portions that had different acquisition geometries and respective geometries were applied. The *Geometry Definition* module was used with appropriate observer, receiver, and source location cards for each of the three portions which included elevations from the GPS data.
3. After each of the geometry steps was completed, the files were merged to create a single data line using the *Seismic Merge*.
4. Noisy files were deleted from the data set.
5. The *Floating Datum Statics* module was used to create receiver and source statics cards. The parameters used were as follows:

Use average CMP elevation	
Consolidated P velocity	400.0
Consolidated S velocity	200.00
Flat datum elevation	1510.00

The *Apply Static Shifts* module used the floating datum cards to apply a shift to the seismic data

6. The *Automatic Trace Editing* module used the default parameters to remove dead or noisy traces.
7. The seismic data was CMP sorted using the *CMP Sort* module.
8. Constant velocity stacks were generated using the *Constant Velocity Stacks* module and the following parameters:

Number of velocities	15
First Velocity	200.00
Last Velocity	700.00
No. of CMP locs/analysis	15
First CMP loc to analyze	100.00
CMP loc increment	50

The rest of the parameters were the defaults. NMO velocities were then picked in Seisviewer.

9. The *Apply Normal Moveout* module was used with a velocity card with the values picked in Seisviewer from step 8.
10. Early mutes were picked in Seisviewer and then *Apply Early Mutes* flow module used the picks as input to apply an early mute with the rest of the parameters the default values.
11. The *Automatic Residual Statics* module created receiver and source static cards. The cards were input into the *Apply Statics Shifts* module with all other parameters the default.
12. An inverse NMO was applied to the data using the exact same parameters as step 9 except the *Do inverse NMO application* is checked.
13. Step 8 is repeated to the residual corrected data with the same parameters and new constant velocities are picked in Seisviewer.
14. Step 9 is repeated with the constant velocities generated from step 13.
15. The *Offset Sort* module with default parameters was used next.
16. The *2-D Dip Moveout* module with a time of interest of 1 was applied.
17. A *Time Variant Bandpass* was applied with the following parameters:

Lo cut	Lo pass	Hi pass	Hi cut
10	20	70	80

18. The *Spherical Divergence Correction* with default parameters was applied.
19. The *CMP Stack* module was applied with default parameters.
20. The CMP stack was migrated using the *Post-Stack Kirchoff Time Migration* module with the NMO velocities generated in step 13 scaled to 75%.
21. Depth conversion using the *Convert time to depth* module with the following parameters was used:

Correction Velocity	450.00
Output depth interval	0.5000
Number of output samples	8000

22. The *Amplitude Equalization* module with default parameters was applied.

Loading data into Kingdom Suite

1. The GPR and SSR data had to be converted to SEG-Y format from SPW format. Conversion was performed in the SPW I/O Utility.
2. To load the radar and seismic data into Kingdom Suite, the *Survey* tab was used and then *Import SEG-Y* was clicked.
3. Choose to import single 2-D (SSR and 2-D GPR) or 3-D surveys (3-D GPR).

4. A new survey was created, *file from disk* was chosen, and the data was imported in the time domain and *Next* was chosen.
5. The survey was given a name when prompted and a description if necessary.
6. *Load the world coordinates* was selected and *File* selected from the drop down menu then the *all files* option was chosen and the text file that contains the GPS data was chosen.
7. *Next* was chosen for the rest of the selections (default selections). On the last page, selection of 8-bit, 16-bit, or 32-bit input of the data can be chosen.
8. A selection screen appears where shot point and receiver associations can be set if Kingdom Suite deems it necessary. However, for this project it was not necessary to input shot points because the software misrepresented the locations.